

Energy Efficient and Adaptive Design for Wireless Power Transfer in Electric Vehicles

Xiaolin Mou, *Student Member, IEEE*, Oliver Groling, and Hongjian Sun, *Senior Member, IEEE*

Abstract—Wireless power transfer (WPT) could revolutionize global transportation and accelerate growth in the Electric Vehicle (EV) market, offering an attractive alternative to cabled charging. Coil misalignment is inevitable due to driver parking behaviour and has a detrimental effect on power transfer efficiency (PTE). This paper proposes a novel coil design and adaptive hardware to improve PTE in magnetic resonant coupling WPT and mitigate coil misalignment, a crucial roadblock in the acceptance of WPT for EVs. The new design was verified using ADS, providing a good match to theoretical analysis. Custom designed receiver and transmitter circuitry was used to simulate vehicle and parking bay conditions and obtain PTE data in a small-scale setup. Experimental results showed that PTE can be improved by 30% at the array's centre, and an impressive 90% when misaligned by 3/4 of the arrays radius. The proposed novel coil array achieves overall higher PTE compared to the benchmark single coil design.

Index Terms—wireless power transfer, magnetic resonant coupling, electric vehicle, power transfer efficiency, misalignment, coil design, adaptive hardware.

I. INTRODUCTION

THE need for a sustainable means of transportation, caused by the depletion of fossil fuels and increase in carbon output severely polluting our environment, has led to a growth in the research and innovation of EV technologies. The available range of conventional EV's is a well-known constraint for customers who are yet to fully adopt eco-friendly motorisation. Furthermore drawbacks, such as large and heavy batteries, high prices and long charging times, are issues which are not easily solved with current battery technology. Since EV's are slowly becoming a more popular choice amongst vehicle owners, especially with government incentives and tax breaks, a more user-friendly means of charging makes economic sense [1]. WPT offers an attractive alternative to a cabled charging system as the driver would simply park their vehicle above a TX coil embedded in the ground, whilst the chassis mounted RX coil initiates charging [2].

According to the range of power delivery, WPT technologies can be divided into far-field WPT technology and near-field WPT technology. Near-field WPT technology can be categorised into two methods: magnetic induction (or inductive power transfer-IPT) and electrostatic induction (or capacitor

power transfer-CPT) [3] [4]. IPT system usually uses helically or flat cooper windings as resonant coils. Foil plates as coupling capacitors for CPT system are potentially more cost effective than complex cooper winding. Moreover, from an alignment perspective, CPT only has one dimension (vertical z axis) [4]. Because of the low value of coupling capacitance, the CPT technology has an average efficiency range between 60-80% and the gap distance is less than 1mm. IPT system not only has vertical z axis dimension but also has dimension in horizontal surface. The gap distance is more than 10 cm.

Another way of classification of WPT technologies is categorising them into three groups, namely inductive coupling WPT, magnetic resonant coupling (MRC) WPT, and electromagnetic radiation-based WPT [5]. MRC-WPT is advantageous with respect to its high safety and long transmission distance [6]. Thus it plays an important role in the design of wireless EV charging systems. There are two interesting fields in WPT for EV applications: static and dynamic charging WPT. For the static scenario, the EV may be charged in a modified car park or garage. In a dynamic WPT system, the EV is continuously charged in a dedicated charging lane using multiple coils embedded in the road [7]. This makes charging more convenient and could result in downsized batteries, reducing their required capacity by 20% and permitting shorter charging times [8] [9].

The key challenge of the WPT technology is its lower transfer efficiency and lower pickup power than the conductive power transmission [10]. It is caused by multiple reasons and much research in recent years has focus on the methods of improving the PTE in EV wireless charging systems. Theodoropoulos *et al.* [11] presented a load balancing control algorithm for EV wireless charging to improve the efficiency. Some research examined different kinds of the primary supply architectures used for EV wireless charging to get the maximum efficiency [12]. Some researchers focused on the new materials, *e.g.*, Y.D. Chung *et al.* proposed a high-temperature superconducting (HTS) resonant coil to improve PTE [13]. The coil structure design and location can also affect the PTE in EV wireless charging [14] [15] [16]. In practice, the most immediate cause in its lower transfer efficiency is its low coupling coefficient of the loosely coupled transformer adapted in the WPT. A bipolar coupler was proposed to improve the coupling [17]. The misalignment between the transmitter and receiver coils can lead to a weak coupling thus reducing the efficiency. Existing WPT technology is bulky and highly sensitive to axial and angular coil misalignment [18] [19] [20] [21] [22] with limitations on the TX and RX coil sizes due to

Manuscript received Month xx, 2xxx; revised Month xx, xxxx; accepted Month x, xxxx.

X. Mou, O. Groling and H. Sun are with the School of Engineering and Computing Sciences, University of Durham, Durham, UK (e-mail: xiaolin.mou@durham.ac.uk, hongjian.sun@durham.ac.uk).

packaging constraints of most vehicles [6].

Recent research explored mitigating techniques such as optimal methods (adaptive rectification, adaptive frequency tuning or adaptive impedance matching [23]) and the arrayed TX coil structures [24] [25] [26]. Although adaptive frequency tuning is widely used in Kilohertz WPT system, the used ISM band is too narrow to accommodate the frequency tracking [27]. This method also needs additional circuitry at the transmitter and receiver [28]. Using impedance matching, the network itself may introduce additional power loss due to unavoidable nonideal capacitors and inductors, and it also leads to increased system complexity [27]. The key benefit of the proposed design of arrayed TX coil structure is that each coil can be individually turned on and off. But there always exists a trade-off between coil size, performance and cost.

For the arrayed TX coil structure, L.C.Meng *et al.* [29] studied two kinds of multicoil format design for the induction cooker. The seven-circle coils structure and the hexagon like seven-coils structure can significantly improve the heating efficiency compared with the traditional single coil induction cooker. A single-layer winding array and coil structure for portable electronic products was presented [30] [31]. Hui and Ho [32] proposed a new multilayer PCB winding structure. Many hexagonal spiral windings were arranged as a transmitter array, and two more layers of PCB winding arrays were added in this design. This invention can successfully solve the problem of charging different types of mobile phone or portable electronic equipment placed on the same charging platform. [33] provided other useful details about WPT system design, particularly the power transmitter and power receiver designs and requirements. Generally, ferrite cores with high permeability and low magnetic loss tangent are useful in the enhancement of the magnetic coupling and consequently leading to high PTE. Hence, the ferrite shielding plays an important role in WPT technologies [31].

The misalignment issue is critical since the electromagnetic energy in conventional MRC-WPT rapidly decays with distance between coils. Lateral and angular misalignment analysis for inductive coupling WPT has been examined by Kyriaki [34]. Previous research was conducted to address the effect of coil design in misalignment scenarios [35] [36] [37], however, no methodology was given to mitigate the issue and no recommendations were made for an economical design to solve the problem once and for all.

To address these challenges, this paper proposes a new coil design and adaptive coil selection hardware. The key contributions are:

- 1) **New method of calculating PTE:** This paper gives a new method for calculating the PTE in laterally misaligned circular coils arrangement. As an important parameter in MRC-WPT technology, the mutual inductance is derived that is different from J. Kim work [38] and X. Zhang *et al.* work [39].
- 2) **Novel EVs charging design:** We first propose the use of the arrayed coil for the static wireless EVs charging. The Seven-TX-Coil array design is proposed that improves the PTE in wireless charging EV systems. These seven TX

coils use the isolated design, where each coil is independent, making the new design convenient for control.

- 3) **Smart coil selection algorithm:** A new smart coil selection algorithm is proposed in this paper. Using this algorithm, only one TX coil of coils array that is nearest to receiver (highest PTE) will be selected to transmit power to the receiver. This design is not only effective in solving the misalignment problem thus keeping higher transfer efficiency, but also can reduce the electromagnetic radiation hazards (*e.g.*, caused by unnecessary electromagnetic field) on drivers' body.
- 4) **The integral hardware prototype:** The integral hardware prototype is developed for evaluating and verifying the new coil array design. XBee RF modules are used for enabling wireless communication. ATmega328 microcontroller is programed to calculate real-time PTE and the OLED can display all necessary data. Moreover, the implementation results fit well with the mathematical theory results and simulation results (under allowable errors and loss).

Section II reviews the theory of MRC-WPT. Section III provides a mathematical method for analyzing the misalignment in MRC-WPT. Section IV presents a novel transmitter coil design which can solve the misalignment problem thus improve the PTE. Section V presents a hardware design and Section VI shows results of simulations and experimental tests.

II. PERFECT ALIGNMENT MRC-WPT MODEL

A two-coil MRC-WPT system consists of a source power, a primary resonant coil (TX), a secondary resonant coil (RX) and a load, as shown in Fig. 1. The subscripts P and Q denote the primary resonant coil and the secondary resonant coil, respectively. S and W denote the source power and load, respectively. D is the distance between the two resonant coils P and Q . The parameter r is the coil loop radius and the parameter a is the wire radius of the resonant coils. Resonant-based WPT enables efficient power transfer over acceptable distances by tuning the capacitive and inductive parameters of both RX and TX circuits to a common natural resonant frequency.

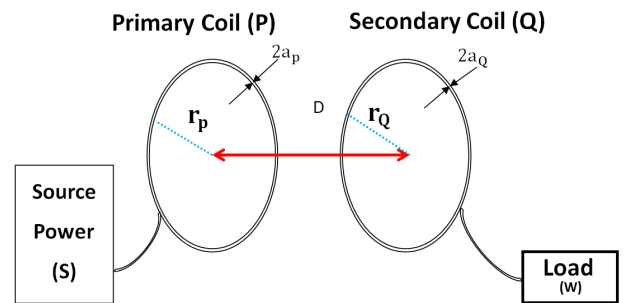


Fig. 1: Block diagram of perfect alignment magnetic resonant coupling WPT

Assuming that the loop radii of the two resonant coils are identical, i.e. $a_P = a_Q$, the self-inductance L , the ohmic

resistance R_o , the radiation resistance R_r , and the capacitance C can be expressed as [40]:

$$L = r\mu_0\mu_r \left[\ln \frac{8r}{a} - 1.75 \right] \quad (1)$$

$$R_o = \sqrt{\frac{\omega\mu_0\mu_r}{2\sigma}} \frac{r}{a} \quad (2)$$

$$R_r = 20 \left\{ \left[\frac{2f\pi}{c} \right]^2 \cdot r^2\pi \right\}^2 \quad (3)$$

$$C = \frac{1}{(2f\pi)^2 L} \quad (4)$$

where μ_0 is the permeability of free space, $\omega = 2\pi f$, μ_r is the relative permeability, c is the speed of light, σ is the conductivity of the conductor and f is the resonant frequency. The total resistance of the resonant coil is $R = R_o + R_r$. (4) indicates that the capacitance C is determined by the self-inductance L of the resonant coil and the resonant frequency f .

According to Biot-Savart's Law, when the centre of the RX resonant coil is aligned with the centre of the TX resonant coil, \mathbf{I} is the current in the TX resonant coil, the magnetic field B can be defined as:

$$B = \frac{\mu_0}{2} \cdot \frac{r_P^2 \mathbf{I}}{(r_P^2 + D^2)^{\frac{3}{2}}}. \quad (5)$$

The mutual inductance M can be given by:

$$M = \frac{\mu_0\pi(r_P r_Q)^2 \mathbf{I}}{2(D^2 + r_P^2)^{\frac{3}{2}}}. \quad (6)$$

The PTE η can be defined as [40]:

$$\eta = \frac{\frac{\Gamma_W}{\Gamma_Q} \frac{K^2}{\Gamma_P \Gamma_Q}}{\left(1 + \frac{\Gamma_W}{\Gamma_Q}\right)^2 + \left(1 + \frac{\Gamma_W}{\Gamma_Q}\right) \frac{K^2}{\Gamma_P \Gamma_Q}} \quad (7)$$

where the PTE η is maximized when $\Gamma_W = \Gamma_Q \sqrt{1 + (K^2/\Gamma_P \Gamma_Q)}$, and can be rewritten as [40]:

$$\eta = \frac{\sqrt{1 + \frac{K^2}{L_P L_Q}} - 1}{\sqrt{1 + \frac{K^2}{L_P L_Q}} + 1} \quad (8)$$

$$\Gamma_P = \frac{R_P}{2L_P}, \Gamma_Q = \frac{R_Q}{2L_Q}, K = \frac{M\omega}{2\sqrt{L_P L_Q}} \quad (9)$$

where Γ is the intrinsic decay rate, K is the coupling coefficient between the two resonant coils and M is the mutual inductance. The final equation of PTE is thus written as:

$$\eta = \frac{\sqrt{1 + \frac{\mu_0^2 \pi^2 (r_P r_Q)^4 \omega^2}{4(D^2 + r_P^2)^3 R_P R_Q}} - 1}{\sqrt{1 + \frac{\mu_0^2 \pi^2 (r_P r_Q)^4 \omega^2}{4(D^2 + r_P^2)^3 R_P R_Q}} + 1} \quad (10)$$

In practice, the size of the TX and RX resonant coils may be different or they are in a misaligned position. The PTE of the misalignment scenario will be given in next section.

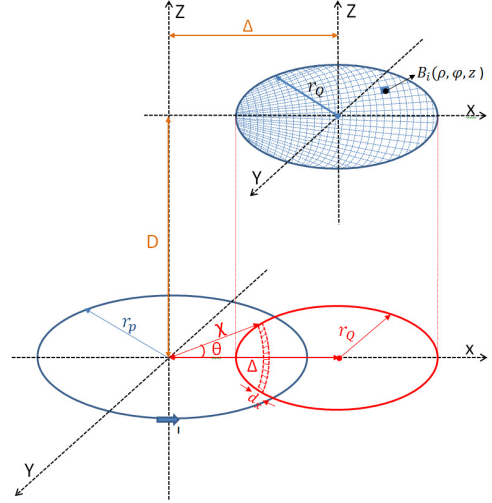


Fig. 2: Illustration of lateral misalignment between coils where r_P is the radius of TX coil, r_Q is the radius of RX coil and Δ is the lateral misalignment distance.

III. MRC-WPT MISALIGNMENT ANALYSIS

In MRC-WPT systems, the power of the TX resonant coil is transmitted to the RX resonant coil through an alternating magnetic field. Numerous experiments have established that the location of two resonant coils can affect the PTE of the whole system.

As proposed by Kyriaki [34], there are two types of misalignment referred to as lateral and angular misalignment. Lateral misalignment involves both horizontal Δ and vertical displacement D in a parallel plane between the centers of the primary and secondary resonant coils, as shown in Fig. 2. In angular misalignment the plane of the RX resonant coil is tilted at an angle ϑ and the coils are coaxial. Since angular misalignment is less likely to occur in a practical EV scenario, this paper only considers the lateral case.

In the case of lateral misalignment, the subdivision magnetic field intensity B_i can be expressed in terms of cylindrical coordinates (ρ, φ, z) . According to Biot-Savart's law, B_i can be written as:

$$B_i(\rho) = \frac{\mu_0 z \mathbf{I}}{2\rho\pi} \cdot \frac{1}{\sqrt{(r_P + \rho)^2 + z^2}} \cdot \left[-F(k) + \frac{r_P^2 + \rho^2 + z^2}{(r_P - \rho)^2 + z^2} \cdot E(k) \right] \quad (11)$$

$$B_i(z) = \frac{\mu_0 \mathbf{I}}{2\pi} \cdot \frac{1}{\sqrt{(r_P + \rho)^2 + z^2}} \cdot \left[F(k) + \frac{r_P^2 - \rho^2 - z^2}{(r_P - \rho)^2 + z^2} \cdot E(k) \right] \quad (12)$$

where ρ and z are displacement in horizontal direction and vertical direction, respectively. φ -directed fields are zero. \mathbf{I} is the current in the TX resonant coil. $F(k)$ and $E(k)$ are the complete elliptical integrals of the first and second kinds, respectively, where k is the modulus. Both equations of the complete elliptical integrals can be given below:

$$F(k) = \int_0^{\pi/2} \frac{d\alpha}{\sqrt{1 - k^2 \sin^2(\alpha)}} \quad (13)$$

$$E(k) = \int_0^{\pi/2} \sqrt{1 - k^2 \sin^2(\alpha)} d\alpha \quad (14)$$

$$k = \sqrt{\frac{4r_P \rho}{(r_P + \rho)^2 + z^2}}. \quad (15)$$

In general, the mutual inductance M can be defined as:

$$M = \frac{N_1 N_2}{\mathbf{I}} \oint_s B_i(z) ds \quad (16)$$

where \mathbf{I} is the current in the TX resonant coil.

As shown in Fig. 2, the RX resonant coil is subdivided into several identical subdivisions and r_Q is its radius. The red circle is the projection of the receiver coil, and it can be divided into several arc areas as magnetic field intensity areas. The magnetic field intensity B_i are same in each arc area, so that we can use integration from $\Delta - r_Q$ to $\Delta + r_Q$ to get the mutual inductance value. The mutual inductance between the TX and RX resonant coil M_{12} can be given by:

$$M_{12} = \frac{N_1 N_2}{\mathbf{I}} \int_{\Delta - r_Q}^{\Delta + r_Q} B_i(z) 2x \arccos \frac{x^2 + \Delta^2 - r_Q^2}{2x\Delta} dx \quad (17)$$

where N_1 and N_2 are the numbers of turns of the TX and RX resonant coils, respectively. In the case of a single loop, $N_1 = N_2 = 1$. x is the distance between the origin of the TX coil and the magnetic field intensity area on the RX coil. This area can be considered as an arc with a width of dx . $B_i(z)$ is the subdivision magnetic field intensity and is given by (12).

M_{12} is a crucial parameter in calculating the PTE of a misaligned MRC-WPT system. The mutual inductance (M_{12}) can be rewritten by some rearrangement of (17):

$$M_{12} = \frac{N_1 N_2}{\mathbf{I}} \int_{\Delta - r_Q}^{\Delta + r_Q} B_i(z) \cdot 2x \sqrt{\frac{r_Q^2 - (x - \Delta)^2}{\Delta \cdot x}} dx. \quad (18)$$

The subsequent equation for PTE can be obtained by substituting (18) into (9) and subsequently into (8), leading to (19) on next page.

IV. NOVEL COIL DESIGN

In order to improve the PTE of MRC-WPT in EV's, a new primary resonant coil array is proposed in this section, which can achieve a higher PTE compared to the traditional single coil benchmark. More importantly, it can solve the misalignment issue.

The proposed coil design consists of a collection of smaller coils arranged in a grid-like fashion across a flat surface as

shown in Fig. 4. A_{1-7} mark the centre of each inscribed circle and represent the TX array coils. The large black circle represents a traditional TX coil. R_P is the radius of the original benchmark coil, and r_P is the radius of the proposed smaller coils. As the RX coil is placed at an arbitrary location above the array, simulating the vehicle's parking misalignment, only the nearest TX coil is energized and transmits power to the EV. To illustrate this, C_{1-n} represent stopping locations at regular intervals from the arrays centre to its outer edge. When the vehicle stops at C_3 , only coil A_2 is energized, for example. This adaptive switching between smaller TX coils, effectively halves the misalignment distance when compared to the larger single coil design.

Please note in this design the cross-coupling between TX coils has not been considered. According to [41] the coupling coefficient is negative when the spacing between adjacent transmitter coils is positive, while the coupling coefficient between nonadjacent transmitters are always negative. If the transmitter coils are overlapping with each other, the cross-coupling should be considered. However, in our design since only one TX will be turned on, we do not need to consider cross-coupling.

As shown in Fig. 4, the array has two possible paths for the RX coil to follow during misalignment, referred to as central and tangential boundaries. If the receiver (EV) stops along the central boundary, the two resonant coils will have the shortest misalignment distance, therefore maximizing PTE. The tangential boundary represents the worst case scenario as it contains a triangular gap where the misalignment distance is at its maximum and thus PTE is reduced.

V. HARDWARE IMPLEMENTATION

These existing EV WPT designs are either too complex, uneconomical, prone to mechanical wear or vulnerable due to potential vandalism. The novel coil array and adaptive hardware design proposed in this paper, reduces coil misalignment and improves PTE, whilst avoiding these problems. The idea is to embed an array of coils in a ground cavity beneath the parking bay surface and control them via custom designed charging circuitry. Using wireless feedback from the vehicle, the parking bay electronics monitor and optimize the PTE of the WPT charging process by selecting the TX coil with optimum alignment to the vehicle mounted RX coil. A system block diagram is shown in Fig. 5.

A recent study of parking behaviour [2] reveals that only 5% of vehicles parked within alignment tolerances for WPT charging can reach at a level of 80% PTE. Perfect alignment can achieve 95% peak efficiency, but the peak efficiency dropped to less than 50% at 15 - 20 cm misalignment. The study showed that drivers were more accurate at parking

$$\eta = \frac{\sqrt{1 + \frac{N_1^2 N_2^2 \omega^2}{\mathbf{I}^2 R_P R_Q} \left(\int_{\Delta - r_Q}^{\Delta + r_Q} B_i(z) \cdot 2x \sqrt{\frac{r_Q^2 - (x - \Delta)^2}{\Delta \cdot x}} dx \right)^2 - 1}}{\sqrt{1 + \frac{N_1^2 N_2^2 \omega^2}{\mathbf{I}^2 R_P R_Q} \left(\int_{\Delta - r_Q}^{\Delta + r_Q} B_i(z) \cdot 2x \sqrt{\frac{r_Q^2 - (x - \Delta)^2}{\Delta \cdot x}} dx \right)^2 + 1}} \quad (19)$$

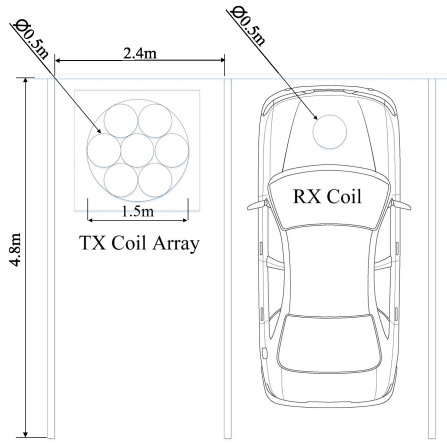


Fig. 3: Proposed parking bay layout illustrating TX coil array (left) and vehicle-mounted RX coil (right).

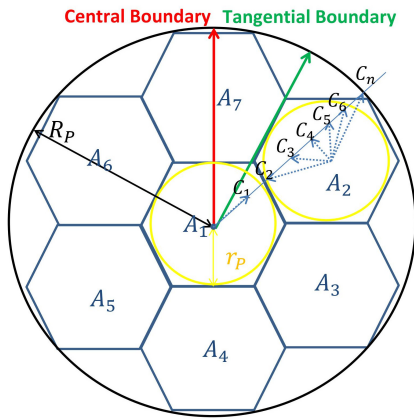


Fig. 4: The proposed TX coil array design

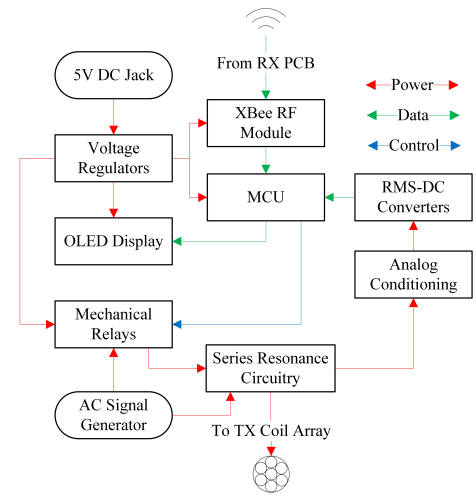
laterally than in the longitudinal direction, most likely by using the sides of the parking bay as alignment guide. Moreover, alignment was superior when drivers were asked to align the front of the vehicle with the charging pad as opposed to the centre, with a mean x-displacement of 0.5 vs. 7.3 cm respectively.

According to [42], the standard space requirements of a typical car park are 2.4 x 4.8 metres with slight variations in the parking bay layout, e.g. parallel, herringbone and in-line designs. Following these recommendations, the outer diameter (\emptyset) of each coil in the proposed array structure is set as 0.5 metres as shown in Fig. 3. The air gap D is 0.2 metres.

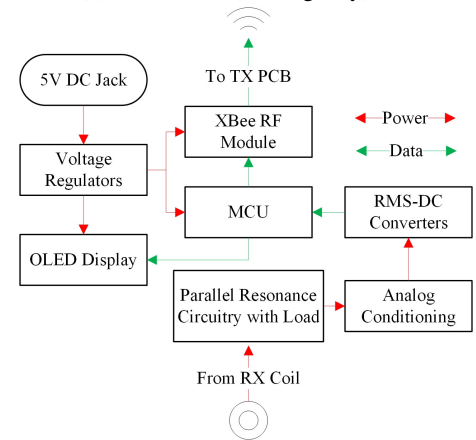
In practice, a 3D printed array structure as shown in Fig. 6 acts as a container and represents a 1:11 scale version of the parking bay equivalent, and the air gap D in practice is 15mm. A small scale lab setup was designed as shown in Fig. 6.

The transmitter consists of the following parts:

- 3D printed array with seven 22 mm radius TX coils;
- 65 mm radius TX PCB coil for benchmark comparison;
- TX PCB (ATMega328 microcontroller, XBee RF module (XBEE2), OLED display, RMS-DC Converter IC's (LTC1968), TX coil connection)



(a) Transmitter (Parking Bay)



(b) Receiver (Electric Vehicle)

Fig. 5: Block diagram of hardware setup using the novel multi-coil array architecture

- 7-channel relay PCB for selecting optimum TX coil.

5V and 3.3V voltage regulators are used to condition the 5V DC jack input and power the ATMega, XBee module, OLED display and RMS-DC Converter IC's. The frequency of resonance is set at 145 kHz (note: the resonant frequency is one of the key factors determining the PTE: in practical setup you might need carefully turn this value first to achieve maximum PTE), which is also used on the signal generator. The voltage amplitude should be in range 0-5Vpp. We then connect the signal generator to the transmitter using the red and black banana plugs.

The receiver consists of the following parts:

- 22 mm radius RX coil without ferrite plate;
- 22 mm radius RX coil with ferrite plate;
- RX PCB (XBee RF module (XBEE2), OLED display, RMS-DC Converter IC's (LTC1968), RX coil connection, 90 Ω resistor (load))

The RX coil is connected to the 2 pin terminal on the receiver PCB. An optimum value of 90 Ω was found by varying the load impedance using a decade resistor until maximum PTE was achieved at 145 kHz (resonant frequency

is key factor of PTE, it maybe has a little difference between this value and practical setup). The load is already set on the RX PCB. There are 2 power plugs, which connect to the TX and PX PCB to power them, then the OLED display should light up on both.

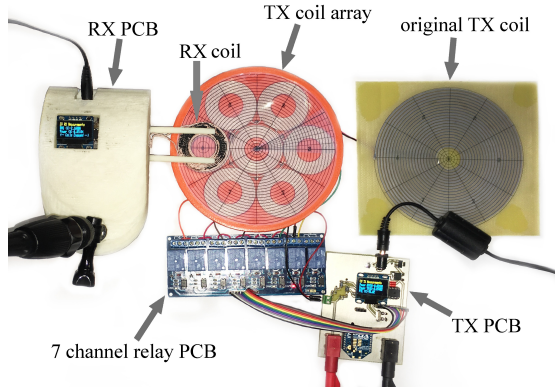


Fig. 6: Small-scale hardware prototype of EV WPT system

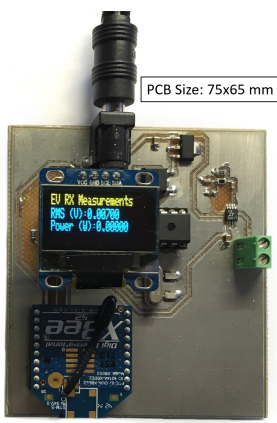


Fig. 7: RX PCB- interface between MRC-WPT circuitry and EV load

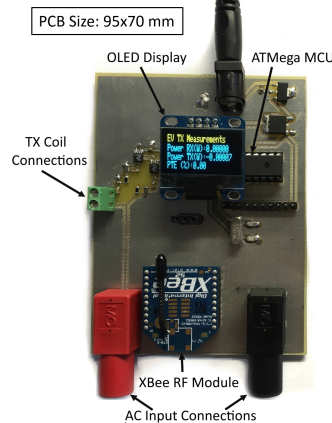


Fig. 8: TX PCB- interface between MRC-WPT circuitry and electricity grid

The vehicle-mounted power receiver measures received power P_{rx} at the load using precision RMS-DC converters, whilst the parking bay transmitter monitors transmitted power P_{tx} . XBee RF modules based on the ZigBee IEEE 802.15.4 protocol are used to establish a wireless feedback loop between the EV and parking bay. An ATmega328 microcontroller (MCU) on the TX side then calculates the current PTE. Embedded software written in C++ iteratively switches power to each of the coils using mechanical relays, until it finds the optimum alignment between TX and RX coils giving maximum coupling - an algorithmic approach.

A. Transmitter Circuitry (Parking Bay)

To simulate a parking bay charging unit and interface to the electricity grid, a two layer TX PCB was designed in EagleCAD to monitor and control the WPT process. A picture of the working prototype can be seen in Fig. 8.

The TX circuitry is composed of four parts:

- i Microcontroller and Wireless communications
- ii Measurement and signal conditioning circuitry

iii Power input and output

iv OLED display and relay outputs

The chosen MCU is an 8-bit ATmega328 clocked at 20MHz. The XBee 802.15.4 module was chosen for wireless communication between RX and TX PCB's, as it integrates seamlessly with the RX and TX pins on the ATmega328. They are typically used for personal area networks (PAN) and provide hardware extensibility for a practical EV scenario, where WPT data, parking space availability and vehicle owner payment information could be exchanged between the vehicle and charging units more efficiently.

Two LTC1968 RMS-DC IC's measure the RMS voltage drop V_{sense} across a 1Ω sensing resistor to give I_T and also across the entire circuit V_s . The MCU then computes P_{TX} .

The measurement and signal conditioning circuitry uses a voltage divider to reduce the signal amplitude to the input range of the RMS-DC converter. A tuning capacitor is connected to the $24 \mu H$ inductive coil in series and parallel for the TX and RX circuits respectively as proposed in Section III. Using (4), a capacitance of 47 nF was calculated to achieve resonance at 145 kHz . A 2-pin screw terminal mounted on the edge of the PCB provides the TX coil connections.

The power rating limitation in this small scale lab setup was 5 W and the traditional series compensation circuit was utilized. The two banana plug connectors took inputs from a standard sine wave generator which has a 60Ω output impedance and simulates the AC power delivered by the electricity grid. A 128×64 OLED display module is connected via I^2C interface to the ATmega328 and provides a GUI to monitor data such as PTE, measured RMS voltages and indicate the currently energized TX coil.

The 5 V mechanical relay PCB uses optocouplers to isolate the high frequency power signal of the waveform generator from the control and signal circuitry on the TX PCB. It is controlled from the ATmega's general purpose input/output (GPIO) pins, and is connected via a ribbon cable attached to the PCB's main Harwin connector.

B. Receiver Circuitry (Electric Vehicle)

To simulate the interface between the battery load of an EV and the MRC-WPT circuitry, a slimmed down version of the TX PCB was designed. A working prototype of the RX PCB can be seen in Fig. 7.

The receiver differs to the transmitter in that it provides feedback of the RX coil location hence allowing the transmitter to adapt to a change in misalignment and select a TX coil with higher PTE. A single RMS-DC converter measures the RMS voltage drop V_{RX} across a 90Ω resistor which represents the load. The MCU then computes P_{RX} in the parallel RLC circuit.

Maximum achievable PTE at resonance depends on the value of load resistance as discussed in [43]. Hence, there exists an optimum load which maximises PTE for a given operating frequency and coupling between coils. An optimum value of 90Ω was found by varying the load impedance using a decade resistor until maximum PTE was achieved at 145 kHz . Table I summarises the electrical and dimensional parameters of both coils.

TABLE I: Parameters of TX coil and RX coil

Property	TX Coil (Array)	Original TX Coil
Inductance (L)	$24\mu H$	$24.47\mu H$
Q-Factor	165	120
No. of Turns & Layers	20 & 1	10 & 1
Inner Radius (r_a & r_o)	10mm	10mm
Outer Radius (R_a & R_o)	22mm	65mm
Turn Spacing (S)	0	0.3mm
Wire Type	Litz Wire	1oz - Cu
Wire or Track Thickness (t)	1.05mm	1.25mm

Property	RX without ferrite plate	RX with ferrite plate
Structure		
Inductance (L)	$23.5\mu H$	$28.8\mu H$

C. Adaptive Coil Control Algorithm

In order to optimise PTE, an adaptive algorithm was programmed in C++ and implemented on the ATmega328 MCU of the TX PCB. The main software requirements to achieve autonomous control were:

- Monitor analogue voltages V_{sense} , V_{TX} , V_{RX} and hence compute P_{TX} and P_{RX} ;
- Send & receive wireless data;
- Operate the mechanical relays;
- Update OLED display with real-time data of selected TX coil, P_{TX} , P_{RX} and PTE .

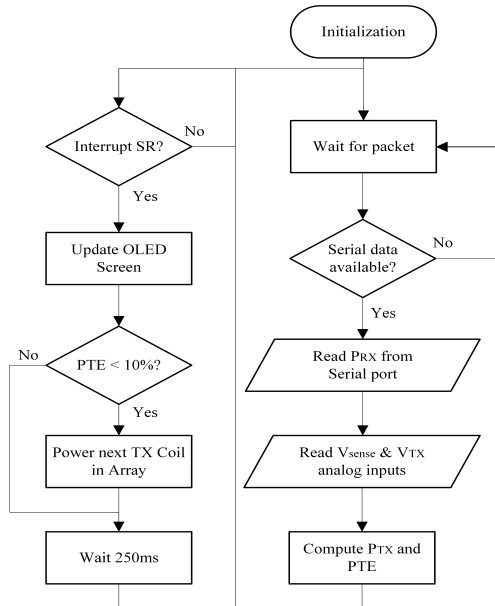


Fig. 9: Adaptive coil selection flowchart

The flowchart in Fig. 9 illustrates the basic operations of the adaptive algorithm. Interrupt service routines are used to refresh the OLED screen every 250 ms and switch between relays if required. If there is a significant drop in PTE, the coil-check algorithm increments to the next coil in the array, until PTE exceeds the minimum 10% threshold. The

relay needs measurement and feedback to choose the TX coil with maximized PTE, because of the random location of the receiver. 10% threshold is chosen as it provides high resolution of measurements after many experimented trials. If this threshold is greater, the relay will be continuously checking status when the receiver coil is at tangential location. Any incoming packets stored in the serial buffer are read and used with measurements obtained from the local analog inputs to compute overall PTE. Finally, the data is displayed on a GUI using a standard OLED display library. Note, the RX PCB code has reduced functionality as it only monitors its analog inputs, displays this info via the GUI and sends serial data via the XBee feedback link to the TX PCB.

VI. SIMULATION & EXPERIMENTAL RESULTS

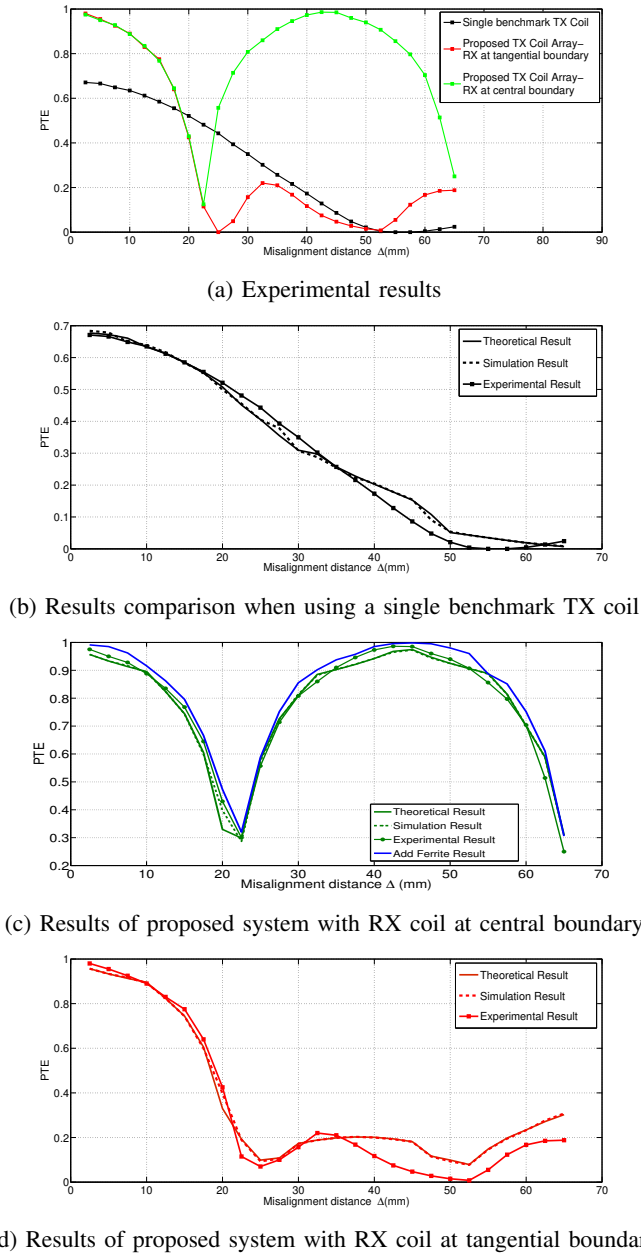
This section evaluates the experimental results from PTE measurements taken for lateral misalignment Δ between the RX coil (without ferrite plate) and TX array structure and compares these to the larger TX benchmark coil. Angular misalignment is neglected as it is unlikely to occur due to the parallel nature of charging coils in a practical EV scenario. In addition, we have performed additional experimental test considering the receiver coil with a ferrite plate in central boundary case. Note that [44] presented a discussion about the different ferrite structures for transmitter coil and receiver coil: when the size of the ferrite plate has the same receiver coil area, it results in higher magnetic field intensity. So in our design, the ferrite plate size is chosen the same as the receiver coil size.

Using the mathematical model for PTE discussed in Section III, and the software package MAPLE16, theoretical PTE values for each point C_n were calculated, where subscript n represents regular points along the radius of the array as shown in Fig. 4. An equivalent circuit of the misaligned MRC-WPT system was then simulated in ADS 2012. The inductance, resistance and capacitance of the resonant coils were calculated using (1), (2) (3) and (4).

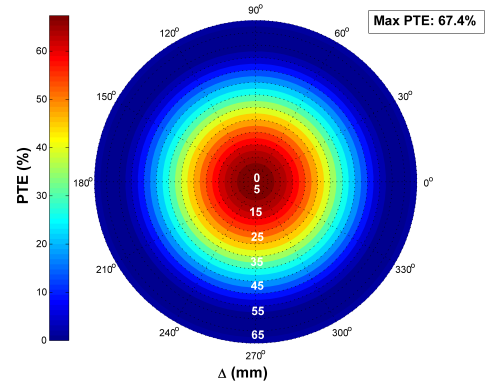
Fig. 10a is the implementation result. The simulated model and small-scale experimental setup used a RX coil radius R_o of 22 mm. The results obtained from experiment broadly agree with the theory and simulations and show that:

- 1) The proposed coil array achieves a higher PTE compared to a single TX coil benchmark in each misaligned position, with an increase of 30% and 90% at the centre and outer edges respectively as shown in Fig.10a.
- 2) The PTE of two peak points in proposed TX coil array can reach 95%, mainly because in these points, the receiver and small transmitter are under alignment location without considering AC/DC conversion. Once AC-DC converters were used on the transmitting side and receiver side rectification and subsequent voltage conditioning for the battery load, this PTE may become lower.
- 3) A "valley" exists in the proposed coil array between $\Delta = 20$ mm and 30 mm, as this is where the RX coil's centre is furthest away from any array coil.

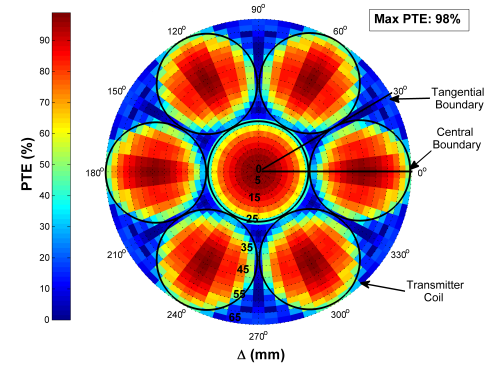
Fig. 10b shows the relation between the PTE and misaligned distance Δ for the original benchmark coil. Fig.10c

Fig. 10: PTE when the misalignment distance Δ varies.

and Fig. 10d show the relationship between PTE and the misaligned distance Δ for the proposed system with the array coil central boundary and array coil tangential boundary in theoretical calculation, simulation and experimental result respectively. The new array design successfully achieved a higher PTE in different scenarios whilst confirming identical trends for PTE vs Δ . We note the theoretical results are lower than the simulation results and experimental results at some points, particularly at misalignment Δ between 15cm to 35cm. This is because these positions are located at the edge of the transmitter coil (the coil winding closely), and the coil winding density is ignored in theoretical analysis. This was also evidenced by [45] which presented the coil winding density can affect the magnetic field intensity of the spiral coil.



(a) Benchmark single TX coil



(b) Proposed TX coil array

Fig. 11: Heat map showing relationship between PTE and misalignment distance Δ when using (a) single benchmark TX coil and (b) the proposed TX array coils. The radius of benchmark TX coil $R_p = 65$ mm and that of the proposed array coil $r_p = 22$ mm.

The practical magnetic field intensity at these positions a little higher than the theoretical calculating value, thus, the PTE is a little higher than theoretical results.

Fig.10c shows the relationship between PTE and the misaligned distance Δ for the proposed system with the array coil central boundary. Additionally, we consider the effects of adding a ferrite plate. In Fig.10c, we can see that compared with the case of receiver coil without ferrite plate, the receiver coil with a ferrite plate can improve the PTE. This is because a ferrite plate is generally useful for enhancing the magnetic coupling, leading to high PTE and low EMF/EML.

For the experimental setup, PTE readings were taken along a horizontal line from the array's centre to its outer radius ($R_o = 65$ mm) in 2.5 mm intervals and were repeated for 0 – 360° at increments of 5°. The vertical displacement (D) between TX and RX coils was kept constant at 1 mm. The results were plotted on a 2D graph and on a heat map using MATLAB.

As shown in the heat map in Fig. 11, the tangential boundary contains a triangular gap between $\Delta = 22.5$ to 30 mm, where the PTE was shown to dip below 15% due to a lower coupling coefficient between TX and RX coils.

The central boundary, however, marks a region where PTE was much higher for any given location of the RX coil along

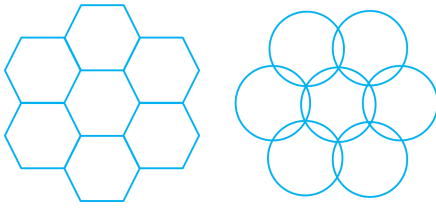


Fig. 12: Future Work of TX coil array design

this line. The heat map shows that the PTE achieved at $\Delta = 45$ mm was 98.5%, whereas the benchmark single coil only achieved 8.5%. Thus an increase of 90% PTE was observed even when the RX coil was misaligned by $3/4$ of the array radius.

VII. CONCLUSIONS AND FUTURE WORK

The success of MRC-WPT in EV's relies on adequate alignment of TX and RX coils, to ensure high PTE and to minimize the losses incurred by both customers and electricity providers. There are many parameters of the coils that affect PTE such as its location, dimensions and geometry. This paper has introduced a novel array-type primary resonant coil design, which solves the misalignment issue in MRC-WPT and achieves a higher PTE. In practice, the coil misalignment is inevitable, since it is difficult for drivers to accurately park their car above a designated charging point or stay within dynamic charging boundaries. Experimental results are obtained using custom designed hardware and have shown a clear match between the theory and real-world implementation of the proposed array design. PTE improvements were observed, of up to 30-90% in the experimental setup. Furthermore, the array design can reduce the RX coil radius and thus reduce the cars weight. Another advantage is the flexibility in choosing any number of TX array coils and varying their arrangement. However, this paper only considers the case where a single TX coil in the array is energized at any time.

In the future we have some further works: 1): the sharp drop in PTE between coils along the tangential boundary could be resolved using an overlapping array or hexagonally shaped coils as shown in Fig. 12. Although the overall array radius in an overlapping configuration would be reduced, the maximum possible misalignment distance between coils would also be reduced. Hence, the red areas marking high PTE on the color map in Fig. 11b would merge together, resulting in an increased average PTE of the array. This would also reduce the slight PTE drop seen at coil transitions along the central boundary. 2): the hardware implementation is a prototype, future work will verify it in high power EV implementation. The adaptive hardware design presented here focuses only on PTE improvements related to the coil misalignment and neglects the losses incurred by additional circuitry required in a complete EV charging system. These might include AC-DC converters on the transmitting side and receiver side rectification and subsequent voltage conditioning for the battery load. Hence the proposed design would need further work to include these functions and to analyze their effects on the overall PTE.

REFERENCES

- [1] T. Essandoh *et al.*, "Chargespot: Wireless power transfer through high resonant frequency," 2014. [Online]. Available: <http://www.eecs.ucf.edu/seniordesign/fa2013sp2014/g20/docs/g20conference.pdf>
- [2] S. A. Birrell, "How driver behaviour and parking alignment affects inductive charging systems for electric vehicles," *Transportation Research Part C: Emerging Technologies*, vol. 58, Part D, pp. 721–731, 2015.
- [3] J. Dai and D. C. Ludois, "A survey of wireless power transfer and a critical comparison of inductive and capacitive coupling for small gap applications," *IEEE Trans. Power Electronics*, vol. 30, no. 11, pp. 6017–6029, Nov. 2015.
- [4] J. Dai and D. C. Ludois, "Wireless electric vehicle charging via capacitive power transfer through a conformal bumper," in *Proc. APEC*, Mar. 2015, pp. 3307–3313.
- [5] Y. Zhang *et al.*, "Frequency decrease analysis of resonant wireless power transfer," *IEEE Trans. Power Electronics*, vol. 29, no. 3, pp. 1058–1063, Mar. 2014.
- [6] X. Mou and H. Sun, "Wireless power transfer: Survey and roadmap," in *Proc. of IEEE 81st VTC*, 2015, pp. 1–5.
- [7] F. Turki *et al.*, "Dynamic wireless ev charging fed from railway grid: Grid connection concept," in *Proc. 2015 International Conference on Electrical Systems for Aircraft, Railway, Ship Propulsion and Road Vehicles*, Mar. 2015, pp. 1–5.
- [8] S. Li and C. Mi, "Wireless power transfer for electric vehicle applications," *IEEE Journal of Emerging and Selected Topics in Power Electronics*, vol. 3, no. 1, pp. 4–17, Mar. 2015.
- [9] J. Shin *et al.*, "Design and implementation of shaped magnetic-resonance-based wireless power transfer system for roadway-powered moving electric vehicles," *IEEE Trans. Industrial Electronics*, vol. 61, Part 3, pp. 1179–1192, 2014.
- [10] S. Y. R. Hui *et al.*, "A critical review of recent progress in mid-range wireless power transfer," *IEEE Trans. Power Electronics*, vol. 29, no. 9, pp. 4500–4511, Sep. 2014.
- [11] T. Theodoropoulos *et al.*, "A load balancing control algorithm for EV static and dynamic wireless charging," in *Proc. 2015 IEEE 81st VTC*, 2015, pp. 1–5.
- [12] B. Esteban *et al.*, "A comparative study of power supply architectures in wireless ev charging systems," *IEEE Trans. Power Electronics*, vol. 30, no. 11, pp. 6408–6422, Nov. 2015.
- [13] Y. D. Chung *et al.*, "Design considerations of superconducting wireless power transfer for electric vehicle at different inserted resonators," *IEEE Trans. Applied Superconductivity*, vol. 26, no. 4, pp. 1–5, Jun. 2016.
- [14] W. Zhang *et al.*, "Loosely coupled transformer structure and interoperability study for EV wireless charging systems," *IEEE Trans. Power Electronics*, vol. 30, no. 11, pp. 6356–6367, Nov. 2015.
- [15] J. Kim *et al.*, "Efficiency of magnetic resonance wpt with two off-axis self-resonators," in *Proc. 2011 IEEE MTT-S International Microwave Workshop Series on Innovative Wireless Power Transmission: Technologies, Systems, and Applications*, May. 2011, pp. 127–130.
- [16] H. Kim *et al.*, "Coil design and measurements of automotive magnetic resonant wireless charging system for high-efficiency and low magnetic field leakage," *IEEE Trans. Microwave Theory and Techniques*, vol. 64, no. 2, pp. 383–400, Feb. 2016.
- [17] J. Deng *et al.*, "Compact and efficient bipolar coupler for wireless power chargers: Design and analysis," *IEEE Trans. Power Electronics*, vol. 30, no. 11, pp. 6130–6140, Nov. 2015.
- [18] Z. Dang and J. Qahouq, "Modeling and investigation of magnetic resonance coupled wireless power transfer system with lateral misalignment," in *Proc. 29th Annual IEEE Applied Power Electronics Conference and Exposition*, pp. 1313–1322, 2014.
- [19] K. Fotopoulou and B. Flynn, "Wireless power transfer in loosely coupled links," *IEEE Trans. Magnetics*, vol. 47, no. 2, pp. 413–430, 2011.
- [20] R. C. Fernandes and A. de Oliveira, "Iterative design method of weakly coupled magnetic elements for inductive power transfer," in *Proc. Brazilian Power Electronics Conference*, pp. 1088–1093, 2013.
- [21] R. Jegadeesan *et al.*, "Overcoming coil misalignment using magnetic fields of induced currents in wireless power transmission," in *Proc. IEEE International Microwave Symposium Digest*, pp. 1–4, 2012.
- [22] M. Q. Nguyen *et al.*, "Field distribution models of spiral coil for misalignment analysis in wpt systems," *IEEE Trans. Microwave Theory and Techniques*, vol. 62, no. 4, pp. 920–933, 2014.
- [23] Y. C. H. Hoang and F. Bien, "Efficiency improvement for magnetic resonance based wireless power transfer with axial-misalignment," *Electronics Letters*, vol. 48, no. 6, pp. 339–341, 2012.

- [24] K. Miwa *et al.*, "Consideration of use of arrayed transmitting coils in wireless power transfer with magnetically coupled resonance," in *Proc. International Symposium on Antennas and Propagation*, pp. 451–454, 2012.
- [25] K. Mori *et al.*, "Positioning-free resonant wireless power transmission sheet with staggered repeater coil array," *IEEE Antennas and Wireless Propagation Letters*, vol. 11, pp. 1710–1714, 2012.
- [26] K. Miwa *et al.*, "A consideration of efficiency improvement of transmitting coil array in wireless power transfer with magnetically coupled resonance," in *Proc. IEEE Wireless Power Transfer*, pp. 13–16, 2013.
- [27] M. Fu *et al.*, "Analysis and tracking of optimal load in wireless power transfer systems," *IEEE Trans. Power Electronics*, vol. 30, no. 7, pp. 3952–3963, Jul. 2015.
- [28] Y. Lim *et al.*, "An adaptive impedance-matching network based on a novel capacitor matrix for wireless power transfer," *IEEE Trans. Power Electronics*, vol. 29, no. 8, pp. 4403–4413, Aug. 2014.
- [29] L. C. Meng *et al.*, "Multicoils design for induction cookers with applying switched exciting method," *IEEE Trans. Magnetics*, vol. 48, no. 11, pp. 4503–4506, Nov. 2012.
- [30] S. Y. Hui, "Planar wireless charging technology for portable electronic products and qi," in *Proc. Proceedings of the IEEE*, vol. 101, no. 6, pp. 1290–1301, Jun. 2013.
- [31] W. X. Zhong *et al.*, "A novel single-layer winding array and receiver coil structure for contactless battery charging systems with free-positioning and localized charging features," *IEEE Trans. Industrial Electronics*, vol. 58, no. 9, pp. 4136–4144, Sep. 2011.
- [32] S. Y. R. Hui and W. W. C. Ho, "A new generation of universal contactless battery charging platform for portable consumer electronic equipment," *IEEE Trans. Power Electronics*, vol. 20, no. 3, pp. 620–627, May. 2005.
- [33] "System description wireless power transfer, volume i : low power, part1: Interface definition." [Online]. Available: <http://www.wirelesspowerconsortium.com>
- [34] K. Fotopoulou and B. Flynn, "Wireless power transfer in loosely coupled links: Coil misalignment model," *IEEE Trans. Magnetics*, vol. 47, no. 2, pp. 416–430, Feb. 2011.
- [35] K. Y. Kim *et al.*, "Power transfer efficiency of magnetic resonance wireless power link with misaligned relay resonator," in *Proc. 42nd European Microwave Conference*, Oct. 2012, pp. 217–220.
- [36] Z. Dang and J. Qahouq, "Modeling and investigation of magnetic resonance coupled wireless power transfer system with lateral misalignment," in *Proc. 29th Applied Power Electronics Conference and Exposition*, Mar. 2014, pp. 1317–1322.
- [37] R. Jegadeesan *et al.*, "Overcoming coil misalignment using magnetic fields of induced currents in wireless power transmission," in *Proc. 2012 IEEE MTT-S International in Microwave Symposium Digest*, Jun. 2012, pp. 1–3.
- [38] J. Kim *et al.*, "Efficiency of magnetic resonance wpt with two off-axis self-resonators," in *Proc. 2011 IEEE MTT-S International IMWS*, May. 2011, pp. 127–130.
- [39] X. Zhang *et al.*, "Coil design and efficiency analysis for dynamic wireless charging system for electric vehicles," *IEEE Trans. Magnetics*, vol. 52, no. 7, pp. 1–4, Jul. 2016.
- [40] H. C. Son *et al.*, "Efficiency analysis and optimal design of a circular loop resonant coil for wireless power transfer," in *Proc. 2010 Asia-Pacific Microwave Conference*, Dec. 2010, pp. 849–852.
- [41] F. Lu *et al.*, "A dynamic charging system with reduced output power pulsation for electric vehicles," *IEEE Trans. Industrial Electronics*, vol. 63, no. 10, pp. 6580–6590, Oct. 2016.
- [42] "Parking standards," Planning Service within the Department of the Environment, Tech. Rep., 2015.
- [43] Vilathgamuwa, "Wireless power transfer for electric vehicles - present and future trends," in *Proc. Electric Vehicles in Smart Grids*. Springer, 2015, pp. 33–60.
- [44] W. Zhang *et al.*, "Loosely coupled transformer structure and interop-

erability study for ev wireless charging systems," *IEEE Trans. Power Electronics*, vol. 30, no. 11, pp. 6356–6367, Nov. 2015.

- [45] M. Q. Nguyen *et al.*, "Field distribution models of spiral coil for misalignment analysis in wireless power transfer systems," *IEEE Trans. Microwave Theory and Techniques*, vol. 62, no. 4, pp. 920–930, Apr. 2014.



Xiaolin Mou (S'17) received the BEng (Hons) degree in electrical engineering from Anglia Ruskin University (U.K.) in 2012 and the MSc degree in satellite communication from University of Sussex (U.K.) in 2013. She is currently working toward the Ph.D. degree in the School of Engineering and Computing Sciences, Durham University (U.K.)

Her research interests include the magnetic resonant coupling wireless power transfer (WPT) for electric vehicles charging, hardware design, control system and renewable energy.



Oliver Groling received his 1st Class MEng (Hons) degree in General Engineering with a specialisation in Electronic Engineering from Durham University (U.K.) in 2016. He has held previous internship positions as Hardware Electronic Engineer at Thales Defence & Space, Electronic Engineering Placement Student working in Formula 1 at Mercedes AMG High Performance Powertrains, and R&D Engineering Intern at Mercedes-Benz. In September 2016 he joined Aston Martin where he is currently working as Electrical Product Development Engineer.

Mr Groling was also presented with an Engineering Leadership Scholarship by the Royal Academy of Engineering (RAENG) in London (U.K.) in April 2014.



Hongjian Sun (S'07-M'11-SM'15) received his Ph.D. degree from the University of Edinburgh (U.K.) in 2011 and then took postdoctoral positions at King's College London (U.K.) and Princeton University (USA). Since 2013, he has been with the University of Durham, U.K., as a Lecturer in Smart Grid. His research mainly focuses on: (i) Smart grid: communications and networking, (ii) Smart grid: demand side management and demand response, and (iii) Smart grid: renewable energy sources

integration.

He is on the Editorial Board of the Journal of Communications and Networks, and EURASIP Journal on Wireless Communications and Networking. He also served as Guest Editor for IEEE Communication Magazine for a Feature Topic: Integrated Communications, Control, and Computing Technologies for Enabling Autonomous Smart Grid, 2016. To date, he has published over 70 papers in refereed journals and international conferences; He has made contributions to and coauthored the IEEE 1900.6a-2014 Standard; He has published five book chapters, and edited two books: IET book "Smarter Energy: from Smart Metering to the Smart Grid" (ISBN: 978-1-78561-104-9), and CRC Book "From Internet of Things to Smart Cities: Enabling Technologies" (ISBN: 9781498773782).